13R.6

3D RADAR DATA DOWNSCALING

Xavier Llort*, Marc Berenguer, Maria Franco, Rafael Sánchez-Diezma, Daniel Sempere-Torres
Grup de Recerca Aplicada en Hidrometeorologia. Universitat Politècnica de Catalunya, Barcelona (Spain)

1. INTRODUCTION

High-resolution three-dimensional precipitation fields are needed for many applications (such to be used as base in radar simulations). The traditional ways of obtaining them are the use of pure stochastic rainfall models, or using real rainfall measurements (usually obtained with a radar) as a base of a downscaling process.

For downscaling techniques, synthesizing rainfall fields with higher resolution than observed, which reproduce the rainfall variability at all scales, is quite a challenge due to the complexities of rainfall (Lanza et al. 2001). First techniques proposed to impose random noise to a given high-quality radar-rainfall field (Krajewski and Georgakakos, 1985). During last decades more advanced downscaling techniques that exploit the fractal behaviour of rainfall have been proposed (see Lovejoy and Schertzer, 1995 and Ferraris et al., 2003 for surveys in this issue).

Among fractal techniques, Perica and Foufoula-Georgiou (1996) proposed a wavelet implementation of a cascade model based on a variability analysis of rainfall at different scales. This technique was later improved in Venugopal et al. (1999) and used in Harris and Foufoula-Georgiou (2001) to evaluate the performance of the *Goddard Profiling* rainfall retrieval algorithm.

Another set of downscaling techniques is based on modelling rainfall fields through the analysis of its Fourier spectrum (see the *Strings of beads* model - Pegram and Clothier, 2001a; 2001b).

Franco et al. (2003) compared both techniques on disdrometer data concluding that, while wavelet technique performs well reproducing the rainfall extremes, it is not able to reproduce the structure of the generated scales. On the other hand, Fourier techniques reproduce well the correlation in the simulated scales but fail to reproduce the extreme values.

In this study we propose a 3D downscaling technique for radar data, based on modelling the precipitation fields using a combination of wavelets, Fourier spectral analysis and homotopic techniques.

2. DOWNSCALING PROCESS

The downscaling technique proposed here is based on three independent steps.

The first one consists on downscaling the first PPI observed by the radar. This is done using a wavelet model combined with a Fourier analysis to downscale up to the desiderated resolution trying to reproduce both, the extreme rainfall values and the field structure.

**Corresponding author address*: Xavier Llort, GRAHI-UPC Gran Capità 2-4 Ed. Nexus D-102. E08034-Barcelona (Spain). e-mail: llort@grahi.upc.edu

Once the first PPI has the proper resolution, the second step consists on downscaling the rest of PPIs through a homotopy of the observed vertical profiles of reflectivity [VPR]. This approach allows us to downscale the upper elevations preserving the original observed radar VPRs.

The last step in the process is the transformation of the dense simulated polar data to the requested cartesian grid.

Radar data used in this study were measured with the C-band radar of the Spanish Meteorological Institute [INM] located in Corbera de Llobregat (close to Barcelona). This radar provides 20-elevation volume scans with 0.9º azimut resolution and 2 km range resolution.

3. 2D WAVELET MODEL

The discrete wavelet transform allows us to study the rainfall field local variability at different scales. In this study, for its simplicity, we have chosen the Haar wavelet base (Figure 1 shows a graphical scheme of its components).

3.1 Scale variability analysis

The 2D Haar wavelet transform decomposes the discrete rainfall field observed at a certain scale (m) in the average component (scaling component, Sc_{m+1}) and three fluctuation components (one in each direction: $Fl_{m+1,1}$, $Fl_{m+1,2}$; and a crossed one: $Fl_{m+1,3}$; see Figure 1 for a graphical scheme and the exact mathematical expression) at the next larger scale ($m+1$). This process can be iterated up to the larger scale possible: the entire rainfall field. In this work, the first fluctuation component corresponds to the variability between azimuts, the second to the variability between ranges, and the third to the crossed variability.

This study has been carried out on a 64 x 64 polar bin area extracted from the radar lowest elevation, and located near the radar in a region not affected by ground clutter.

The proposed wavelet model is based on the fact that sample distributions of the standardized fluctuations of the reflectivity factor ($mm^6 \cdot m^{-3}$): $X_{m,i}$, are Gaussian distributed with zero mean and standard deviation following a simple scale-law (Perica and Foufoula-Georgiou, 1996):

$$X_{m,i} = \frac{Fl_{m,i}}{Sc_m} \sim N(0, \sigma^2_{m,i}) \qquad (1)$$

Concretely, the standard deviation decays with a power-law over successive fines to coarse scales:

$$\sigma_{m,i} \propto 2^{(m-1)\cdot H_i} \sigma_{1,i} \qquad (2)$$

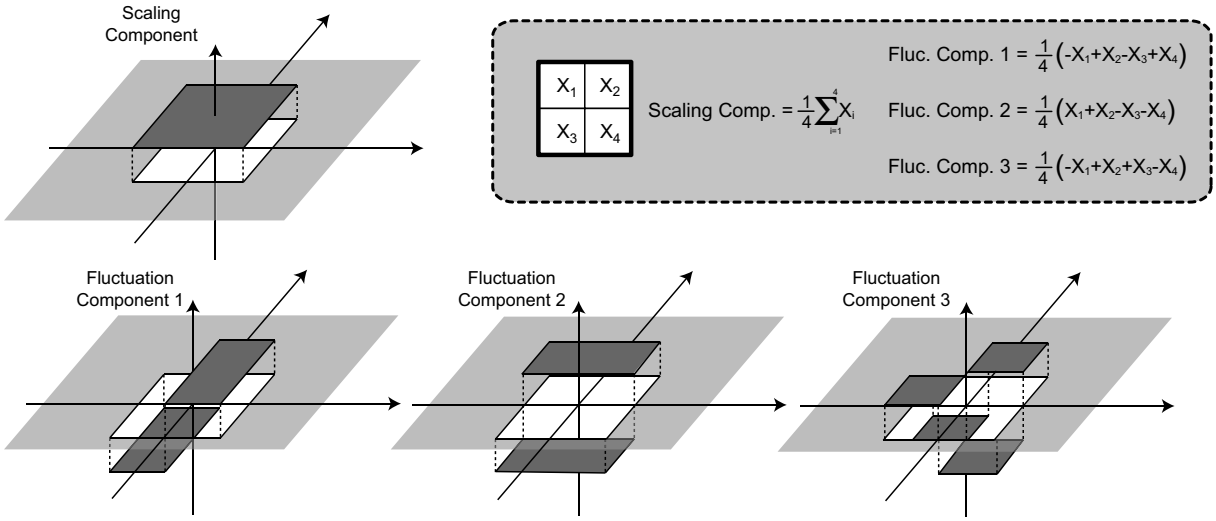

Fig. 1. Graphical scheme and mathematical expression of the 2D Haar wavelet base components.

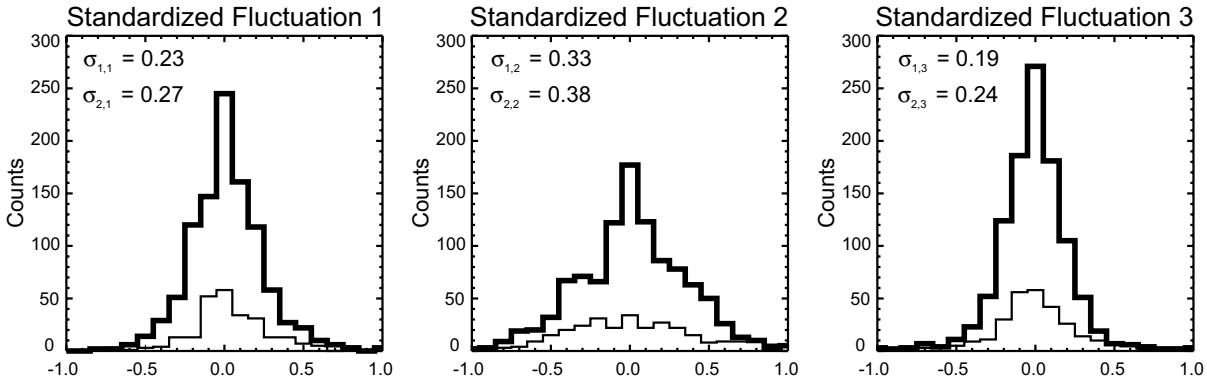

Fig. 2. Standardized fluctuations sample distribution in a stratiform case for two consecutive scales. Thick line corresponds to the scale *m=1* and thin line to *m=2*.

Equation 2 relates the standard deviation at each scale with the one at the smallest observed scale (*m=1*), where H_i are the parameters of three scaling laws fitted to the standard deviations of the three standardized fluctuations ($X_{m,i}$) at different scales.

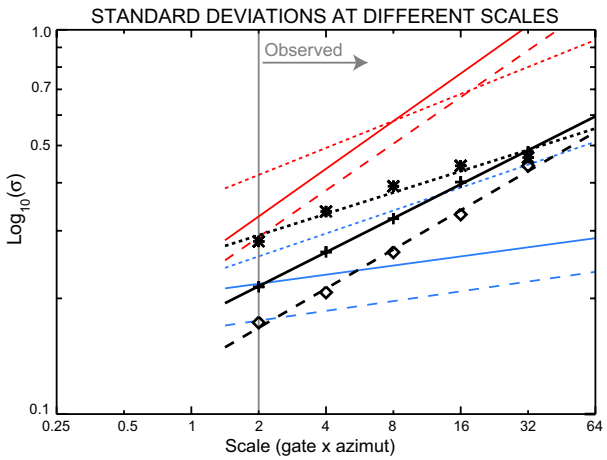

Fig. 3. Standardized fluctuations standard deviation at various scales for three cases: convective (red), stratiform (blue) and an average of 100 images containing a mix of cases (black). Different lines correspond to the three fluctuations: FI_1, (solid), FI_2 (dotted) and FI_3 (dashed).

Figure 2 shows the sample distributions of the three standardized fluctuations at two consecutive scales for a stratiform case not affected by bright band. It should be noted that increasing the scale results in reducing the number of samples by a factor of 4. Therefore, the number of samples of the second scale-up distributions (*m=2*) is smaller that in the first scale (*m=1*).

Figure 3 shows the standard deviations of the three standardized fluctuations over several scales for two different radar images (convective and stratiform) and for 100 images containing a mix of cases. It can be observed, for all the fluctuations, that the convective case has higher values of H_i (in Eq. 2) than the stratiform case. The average of several images performs between those two cases. Thus, different power-laws depending on the image characteristics should be taken into account.

3.2 Downscaling process

The downscaling process consists on, once the scale variability analysis is done, perform the inverse wavelet transform with the proper fluctuations.

So, the first step consists on extrapolating the standard deviations of the three standardized fluctuations at the current scale, from the experimental power-law (Equation 2).

Once we have the standard deviations, we generate random fields Gaussian-distributed with zero-mean and the appropriate standard deviation. To avoid obtaining negative reflectivity values in the final result, Gaussian distributions are truncated between –1 and 1. These generated fields will correspond to the three standardized fluctuations at the current scale.

The next step is obtaining the fluctuation values from Equation 1, that is, multiply the standardized fluctuation components by the scaling component to undo the standardization. Finally, simulated reflectivity values are obtained solving the linear system of equations written in Figure 1.

If the size of the area to downscale is not a power of two (requisite for the Haar wavelet model) it is extended up to the next power with zeros and, after the wavelet process, cut back to the required size. The whole process can be iterated up to the requested resolution.

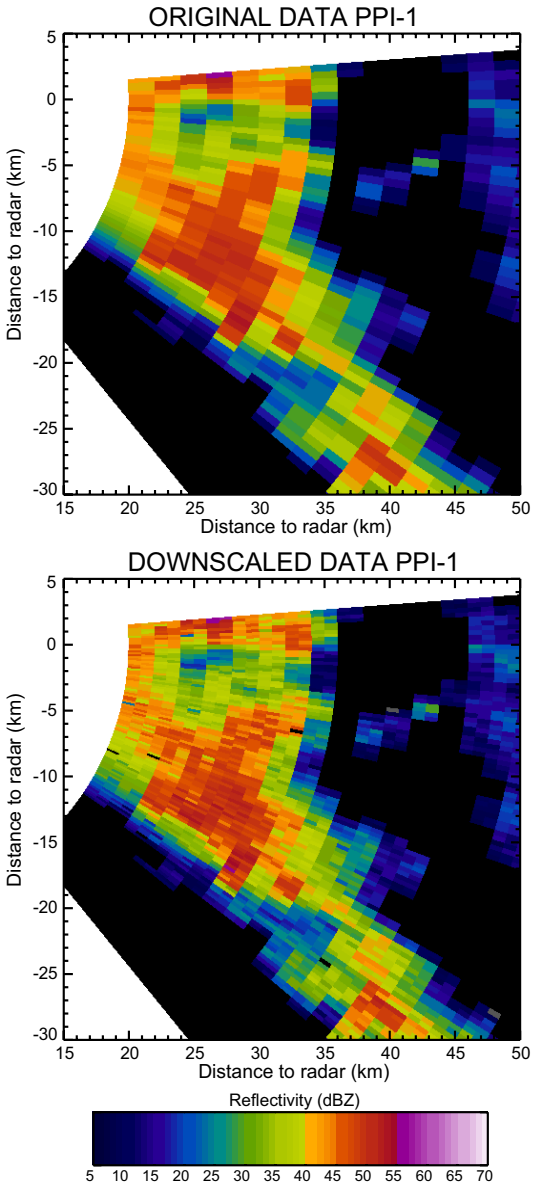

Fig. 4. Downscaling of the first radar PPI iterating once the wavelet process.

Figure 4 shows an example of this downscaling process, iterating once, over a section of a convective sitiation. The fluctuation variance power-laws used for this example are experimentally obtained from a dataset of 100 images. In this figure it can be appreciated how, preserving the observed pixel structure, the method introduces new extreme rainfall values.

4. FOURIER ANALYSIS OF DOWNSCALED FIELDS

The main problem of the wavelet downscaling technique described above is that no correlation between the new generated pixels is taken into account. That implies that when we analyze the Fourier spectra of the downscaled fields, the high frequency components change respect the ones that real rainfall would have.

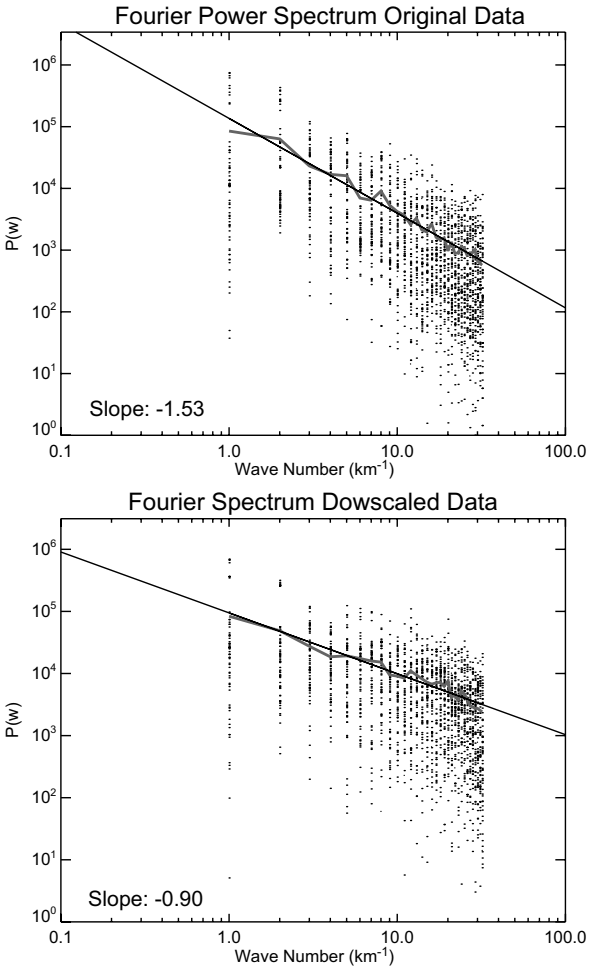

Fig. 5. Fourier power spectrum radially averaged for a stratiform image (up), and for the same imaged downscaled (2 iterations form the images averaged 2 scales-up) plotted in logarithmic scale. The grey line represents the mean radially averaged spectrum and the line its best fit. The slope of that line is plotted inside each graph.

In order to study how the different methods perform over the Fourier spectrum of the downscaled image, we first have averaged the radar images two scales up, and after applied two iterations of the technique to reach the original resolution. Thus we can compare the original spectrum against the

obtained after the downscaling and decide which technique is able to reproduce better the original correlation at lower scales. The comparison skill used is the slope of the best linear fit to the logarithm of the power spectrum (the radially averaged power spectrum derived from the fields is supposed to follow a power-law in frequency, see Pegram and Clothier, 2001a; 2001b):

$$\Gamma(f) \propto f^{\beta} \tag{3}$$

Figure 5 shows the radially averaged Fourier power spectrum for a stratiform image and for the same image downscaled (with two iterations starting from the image upscaled two iterations). Mean spectrum is plotted with its best fit for both graphs. In this figure it can be seen how, after the downscaling process, the slope becomes more close to zero (less correlation between pixels).

The first step to improve this issue was proposed by Harris and Foufoula-Georgiou (2001), who performed a sorting of the rain values generated within a pixel to improve connectivity. The sorting is done in each wavelet iteration by shifting the high value to the place surrounded by higher values and the lowest to the place surrounded by lower values. This pixel sorting succeeds in recovering part of the lost structure in the downscaling process, but not all.

In order to make another step in this direction, we studied the power spectrum of the observed standardized fluctuations in each scale. The main idea is not only simulate the right distribution of the standardized fluctuations when downscaling, but also their internal structure. So, in each observed scale we assume that Equation 3 can also represent the power spectrum of standardized fluctuations.

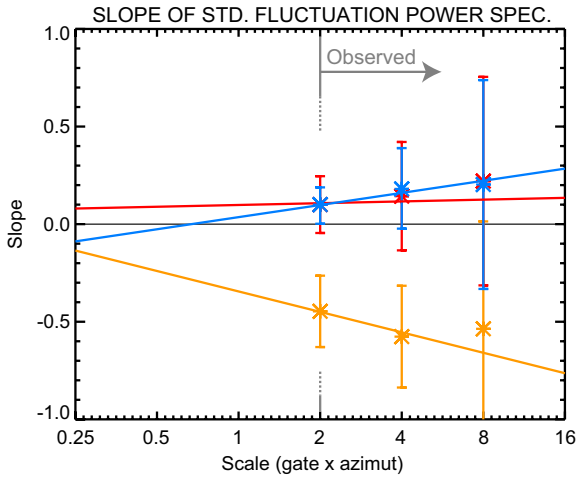

Fig. 6. Power spectrum slope of the three standardized fluctuations (FI_1 in orange, FI_2 in red and FI_3 in blue) at the various scales based on 100 rainy images containing a mix of cases. The asterisks correspond to the mean and the bars the 1-σ interval.

Figure 6 shows the slope of the standardized fluctuations radially averaged power spectrum at various scales for 100 rainy images. This figure shows how, while the FI_2 and the FI_3 perform close to zero in the positive side, FI_1 performs in the negative side. Using the best linear fit we can extrapolate the slope of the Fourier power spectrum of the standard fluctuations to the new scales. These slopes are introduced in the generation of the Gaussian-distributed fluctuations using a power-law filter.

Both techniques (pixel sorting and imposition of a concrete Fourier spectrum to the standardized fluctuations) agree with the downscaling philosophy: the observed scales do not change after the process.

The slopes of the Fourier power spectra obtained through the various techniques are summarized in Table 1 for a stratiform image and a convective one. In both cases it can be seen that imposing the structure to the standardized fluctuations and performing the pixel sorting results in obtaining slopes corresponding to fields with more correlation at small scales.

TABLE 1. Slope of the radially averaged Fourier power spectrum for a stratifom case and a convective case.

Technique	Strat.	Conv.
Original Image	-1.53	-1.61
Wavelet Dowscaling [WvD]	-0.90	-1.51
WvD + Pixel sorting	-0.98	-1.64
WvD + Fluc. spec. structure	-0.92	-1.54
WvD + Fluc. spec. structure + Pixel sorting	-1.00	-1.67

In order to visually show the effect of imposing structure when downscaling, Figure 7 shows an example of downscaling of the first radar PPI with two iterations starting form the data upscaled two iterations. The lower-left plot shows the result of only applying the wavelet technique, and the lower-right plot applying also the pixel sorting and imposing structure to the standardized fluctuations. From a qualitative point of view it can be observed that, when imposing structure, the result is closer to the original rainfall field.

5. 3D DOWNSCALING

Once the first radar PPI is downscaled up to the desiderated resolution it is used to downscale the rest of PPIs through a homotopy of the original observed VPRs. The reasons of not downscaling each PPI using the technique explained before are that the observed VPR will be destroyed due to the random component of the process. Moreover, the homotopy technique allows us to create “artificial” elevations between the observed ones. This last property would allow us to increase the vertical density of the values far from radar and thus, improving the results in the transform to cartesian values.

5.1 VPR Homotopy

To calculate the simulated reflectivity value in a concrete point when downscaling of the upper elevations, first we we obtain the VPR at this point. To do this, we perform a linear homotopy of the observed VPRs surrounding that point (see Figure 8 for a graphical scheme). The original VPRs are considered to be piece-linear functions of the observed values and, for the homotopy, they are normalized by their value in the first elevation.

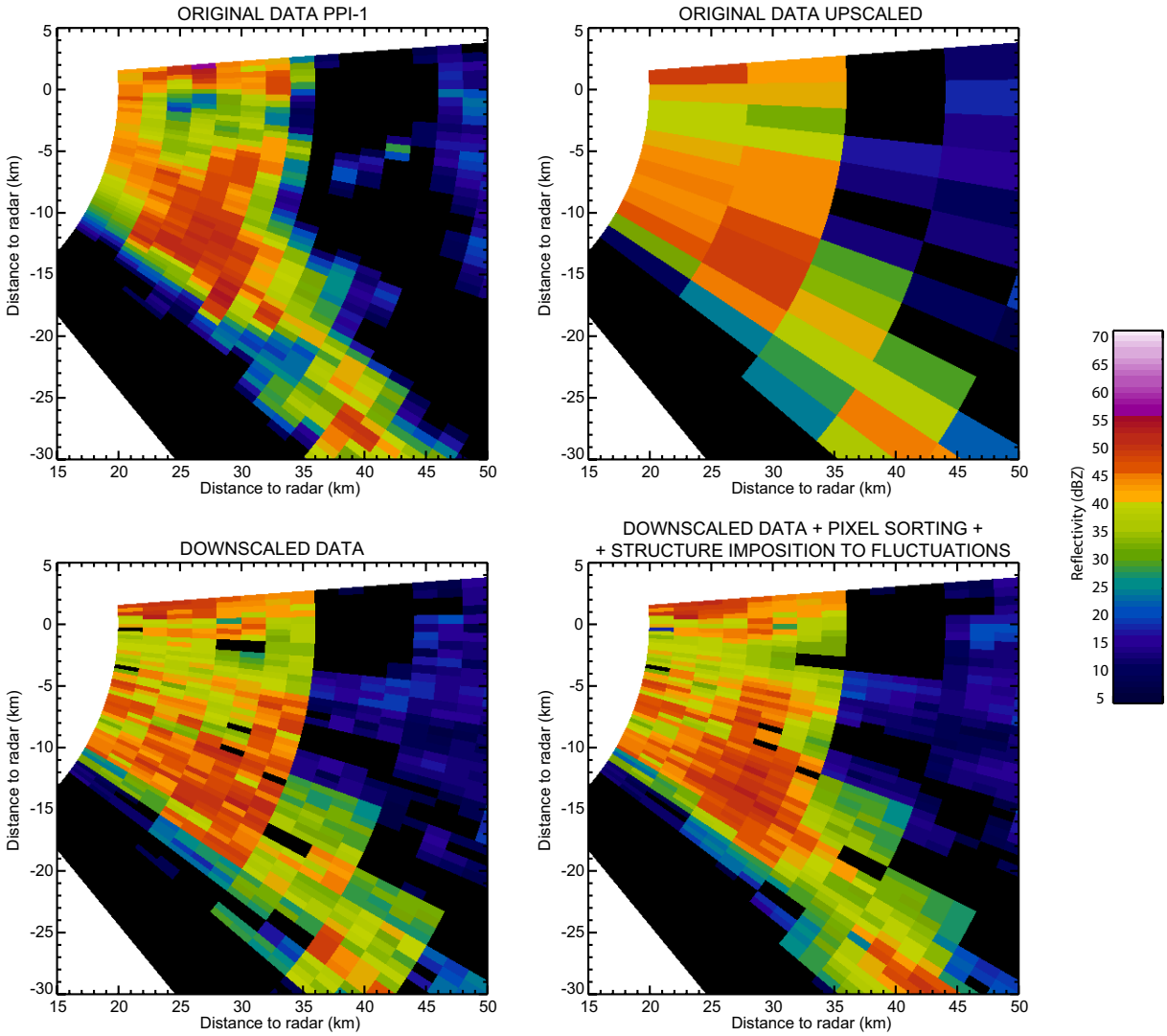

Fig. 7. Downscaling example. The upper plots represent the original data (left) and the original data upscaled two iterations (right). The second row graphs represent the fields obtained after two wavelet iterations (left) and after two wavelet iterations, imposing structure to the standardized fluctuations and performing a pixel sorting (right).

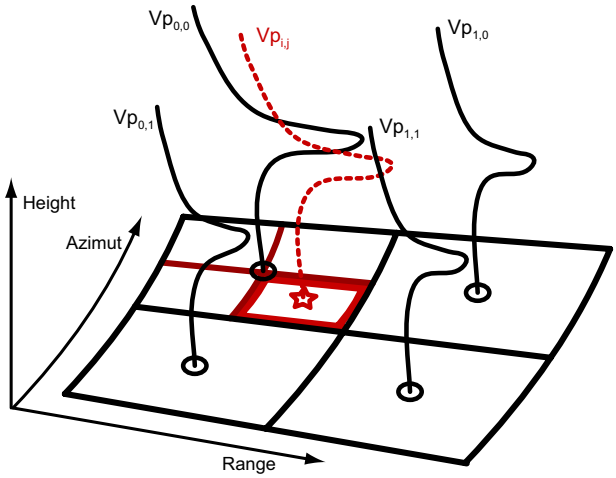

Fig. 8. Homotopy scheme. The points marked with a circle correspond to the original data and their profiles are the black ones. The red point (star) is the obtained through 2D downscaling of the first PPI and its vertical profile (dashed-red) is the obtained through homotopy.

Mathematically, the homotopy is defined as follows:

$$G:[0,1]^2 \times H \longrightarrow C(H)$$
$$(i,j,h) \longrightarrow G(i,j,h) = Vp_{i,j}(h) \tag{4}$$

Where H are the heights, $[0,1]^2$ is 2D unit interval, base for the homotopy, $C(H)$ denotes the continuous functions in height (the vertical profiles) and $Vp_{i,j}$ is defined as:

$$Vp_{i,j}(h) = \left\{ i \cdot Vp_{1,0}(h) + (1-i) \cdot Vp_{1,0}(h) \right\} \times (1-j) + \\ + \left\{ i \cdot Vp_{1,1}(h) + (1-i) \cdot Vp_{0,1}(h) \right\} \times j \tag{5}$$

Where $Vp_{0,0}$, $Vp_{0,1}$, $Vp_{1,0}$ and $Vp_{1,1}$. are the observed profiles surrounding the point of interest, normalized by their value at the first elevation. With this process, for each point inside the $[0,1]^2$ interval, we can find a normalized VPR, function of the surrounding VPRs and the position of that point. The i and j index are calculated as linear function of its position inside the interval. In particular the homotopy recovers the original normalized profiles in the interval

extremes, that is, $G(0,0,\cdot)=Vp_{0,0}$, $G(0,1,\cdot)=Vp_{0,1}$, $G(1,0,\cdot)=Vp_{1,0}$ and $G(1,1,\cdot)=Vp_{1,1}$.

Once we have calculated the normalized VPR at the desiderated point, we undo the normalization using the downscaled value of the first elevation at the point of analysis, and we take the value in the corresponding height. This will be the downscaled pixel value in that elevation. The same process can be used to create "artificial" elevations between the observed ones.

Figure 9 shows the downscaled fields obtained through this technique when applied to two different upper PPIs. The downscaled first PPI used (base for the homotopy) is the shown in Figure 7 (down-left). It can be observed that the homotopy re-introduces the variability lost when averaging.

The introduction of a random component in the VPRs obtained from the homotopy is under investigation.

5.2 Polar to cartesian transformation

The last step of the 3D downscaling process is the transform of the downscale polar values into the requested cartesian grid. This step is done by the "nearest neighbour" algorithm in order to preserve the generated extreme values in the downscaling process and the small-scales variability (Trapp and Doswell, 2000).

6. CONCLUSIONS

In this work a 2D downscaling technique based on a wavelet model is presented. This technique is able to reproduce the extreme values of the rain (like usual wavelet models) and, at the same time, improve the correlation between the generated values in the new scales.

The 2D dimensional downscaling process is complemented with a vertical homotopy of VPR in order to obtain a complete 3D downscaling algorithm. This vertical downscaling does not destroy the vertical profiles of reflectivity measured by the radar and allows us to increase the vertical values density.

This study has been done in polar data, which implies that not all the pixels have the same area. Therefore, the standard deviations obtained at the different scales for the wavelet downscaling will change depending on the distance to the radar of the pixels used for its calculation. Further investigation of this issue is required.

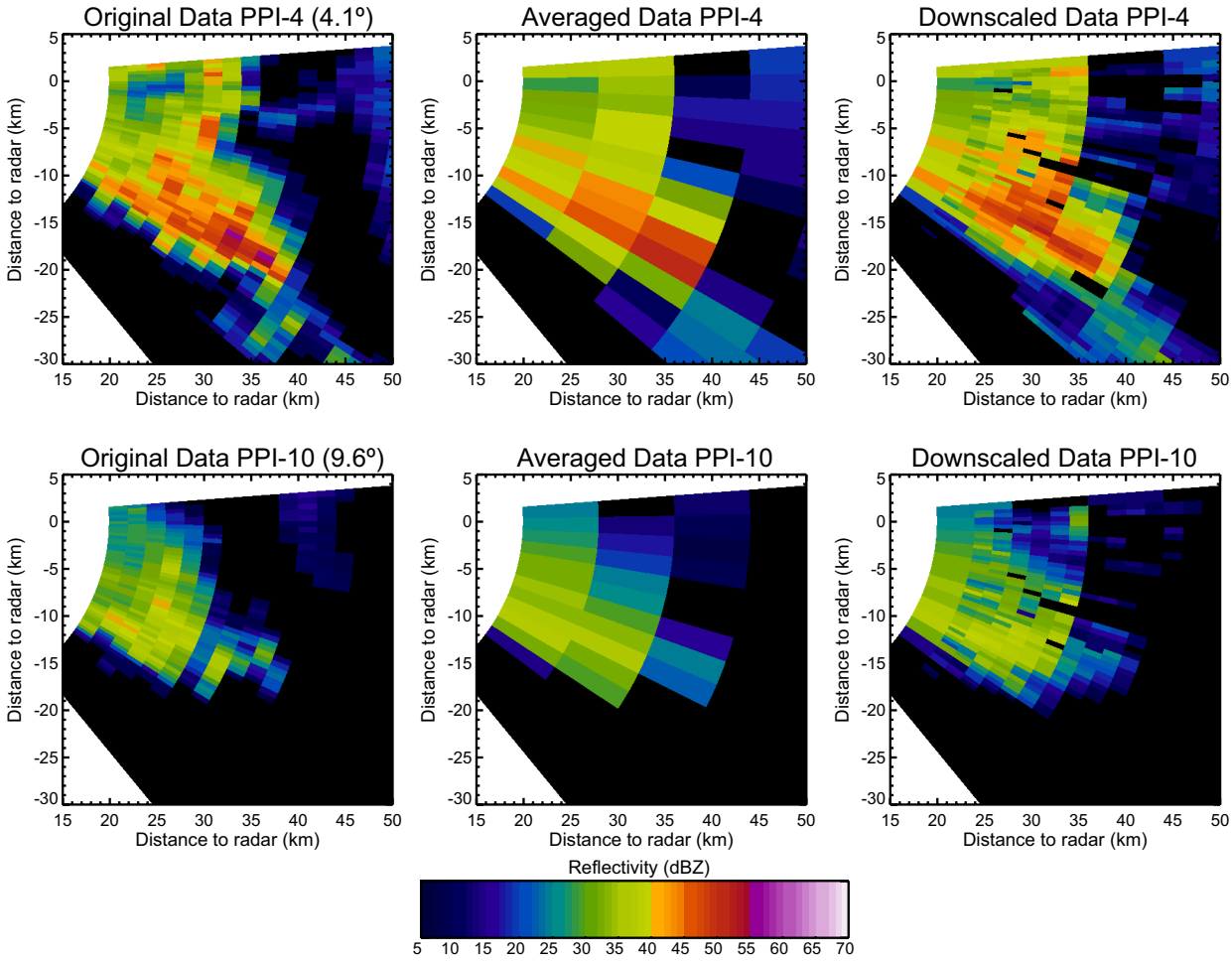

Fig. 9. Downscaling of the upper elevations example. The first column represents the original data at two different elevations (4.1º and 9.6º), the second column the same data averaged two scales up, and the third column the result of the 3D downscaling technique.

Future work will include an extended study of how to improve the results of the 2D downscaling model to reproduce the spectrum of the fields. The introduction of a random component in the vertical downscaling will be also investigated.

Acknowledgements: This project has been carried out in the framework of the EC projects VOLTAIRE (EVK2-CT-2002-00155) and FLOODSITE (GOCE-CT-2004-505420). Radar data were provided by the Spanish Institute of Meteorology (INM).

References

Ferraris, L., S. Gabellani, U. Parodi, J. von Hardenberg and A. Provenzale, 2003: Revisiting multifractality in rainfall fields. *J. Hydrometeor*. **4**(3). 544-551.

Franco, M., I. Zawadzki and D. Sempere-Torres, 2003: A comparative study of different rainfall downscaling processes. Preprints, *31th Conf. on Radar Meteorology*, Seattle, WA, Amer. Meteor. Soc., 285-286

Harris, D. and E. Foufoula-Georgiou, 2001: Subgrid variability and stochastic downscaling of modeled clouds: Effects on radiative transfer computations for rainfall retrieval. *J. Geophys. Res.* **106**(D10). 10349-10362.

Krajewski, W. and K. Georgakakos, 1985: Synthesis of radar rainfall data. *Water Resour. Res*. **21**(5). 764-768.

Lanza, L. G., J. A. Ramírez and E. Todini, 2001: Stochastic rainfall interpolation and downscaling. *Hydrol. Earth System Sci.*, **5**(2), 139-143.

Lovejoy, S. and D. Schertzer, 1995: Multifractals and rain. *New uncertainty concepts in hydrology and hydrological modeling*. Cambridge Press. 62-103.

Pegram, G. G. S. and A. N. Clothier, 2001a: High resolution space-time modeling of rainfall: the "String of Beads" model. *J. Hydrol*. **241**. 26-41.

——, 2001b: Downscaling rainfields in space and time, using the String of Beads model in time series mode. *Hydrol. Earth System Sci*, **5**(2), 175-186.

Perica, S. and E. Foufoula-Georgiou, 1996: Model for multiscale disaggregation of spatial rainfall based on coupling meteorological and scaling descriptions. *J. Geophys. Res*. **101**(D21). 26347-26361.

Trapp, R. J. and C. A. Doswell, 2000: Radar data objective analysis. *J. Atmos. Oceanic Technol*. **17**(2). 105-120.

Venugopal, V., E. Foufoula-Georgiou and V. Sapozhnikov, 1999: A space-time downscaling model for rainfall. *J. Geophys. Res*. **104**(D16). 19705-19721.